Korean J. Chem. Eng., 37(8), 1331-1339 (2020)
DOI: 10.1007/s11814-020-0570-x

pISSN: 0256-1115
eISSN: 1975-7220

Glass ceramic coating on $LiNi_{0.8}Co_{0.1}Mn_{0.1}O_2$ cathode for Li-ion batteries

Hyeong Seop Kang, Palanisamy Santhoshkumar, Jae Woo Park, Gyu Sang Sim, Murugan Nanthagopal, and Chang Woo Lee†

Department of Chemical Engineering & Center for the SMART Energy Platform, College of Engineering, Kyung Hee University, 1732 Deogyeong-daero, Giheung, Yongin, Gyeonggi 17104, Korea
(*Received 30 September 2019 • Revised 28 March 2020 • Accepted 11 May 2020*)

Abstract−Alleviating the surface degradation of Ni-rich cathode materials is desirable to achieve better electrochemical performance. Herein, we report the surface coating of lithium diborate (Li_2O-$2B_2O_3$) over the Ni-rich $LiNi_{0.8}Co_{0.1}Mn_{0.1}O_2$ (NCM811) cathode material and the systematic investigation of its electrochemical properties. The structural and morphological properties were characterized through X-ray diffraction (XRD), high resolution field-emission scanning electron microscopy (HR FE-SEM), and high resolution field-emission transmission electron microscopy (HR FE-TEM). As a cathode material for Li-ion batteries, the 1.0 wt% Li_2O-$2B_2O_3$ coated NCM811 exhibits better electrochemical properties than the bare NCM811 as well as 0.5 and 2 wt% coated electrodes at room and elevated temperatures (60 °C). The improved electrochemical performance of 1.0 wt% Li_2O-$2B_2O_3$ coated NCM811 might be due to the optimal coating amount that promotes better ion and electron movement along with prevention of surface degradation.

Keywords: Lithium Diborate, Cathode, Ni-rich, Wet Chemical, Surface Modification

INTRODUCTION

The development of energy-dependent devices for the various needs of modern society has facilitated considerable research in the field of energy sources. Lithium ion batteries (LIBs) have been mostly used in a variety of electronic devices such as mobile phones, laptop computers, and cameras [1-5]. These types of secondary batteries will be key players for automobile applications in the upcoming years because of their high energy and high power density when compared to other types of rechargeable batteries [2,6]. In the LIB industry, $LiCoO_2$, for example, has been broadly used as an auspicious contender for commercial applications [7,8]. Nevertheless, the toxicity and cost of cobalt restrict its use in further development processes. In addition, problems like rapid capacity fading, which lead to the poor cycling performance of $LiMn_2O_4$, are due to the John-Teller effect [9-11]. Therefore, numerous attempts have been made to develop cathode materials to improve the performance of LIBs.

Due to its high theoretical capacity of around 275.5 mAh g^{-1}, low cost, and environmentally friendly nature, Ni-rich layered oxide $LiNi_{0.8}Co_{0.1}Mn_{0.1}O_2$ (NCM811) material has been considered as a promising cathode active material candidate [12-16]. However, NCM811 has problems, including thermal degradation of electrode material, especially at elevated temperatures, which results in poor cycling performance [17,18]. When the reaction proceeds, unstable Ni^{4+} on the surface of the NCM811 material is reduced to Ni^{2+}, which causes phase change of the electrode material [19,20]. As a result, lithium ion diffusion is prevented, followed by capacity fading. Therefore, the prevention of side reactions such as electrolyte decomposition, HF attack, dissolution of metal from the electrode material into the liquid electrolyte, and controlling the surface impurities of the electrode surface are essential for the application of Ni-rich layered electrode materials in rechargeable LIBs [21].

To overcome these problems, surface modification or coating on Ni-rich oxide materials is an effective approach which can act as an artificial physical layer. In most cases, carbon-based materials such as graphene oxides (GO) [22], reduced graphene oxides (rGO) [23], and single/multi-walled nanotubes, metal oxides such as V_2O_5 [24], CuO [25], CaO [26], ZrO_2 [27], and metal fluoride-like LiF [28], and metal phosphates such as $AlPO_4$ [29] are used as the coating materials on Ni-rich cathode electrode materials to prevent the core material from unwanted SEI layer formation. Herein, we utilized lithium diborate (Li_2O-$2B_2O_3$) glass ceramic oxide with the major advantage of good ionic conductivity to make a protection layer on Ni-rich cathode materials [30]. Li_2O-$2B_2O_3$ consists of a Li_2O network modifier and B_2O_3 as a glass network former. When assembling Li_2O-$2B_2O_3$ units, respective units of B_2O_3 and Li_2O contain bridging oxygen atoms and B_2O_3 help to build the glass ceramic oxide with Li_2O [31]. Some oxygen atoms show negative charges and retain the cations of Li_2O. Thus, the anions are fixed to the covalent bonds but alkali cations are weakly bonded to the non-bridging oxygen atoms due to columbic interactions [32]. Therefore, we believe that alkali cations are easy to move through the Li_2O-$2B_2O_3$ layer with an increase of the ionic mobility. Fig. 1(a) shows a schematic of the Li_2O-$2B_2O_3$ glass ceramic oxide structure. Through the network composed of BO_3 and BO_4^-, lithium ions can move to the inside of the network. The structural change of the network is explained by the following reaction:

$$BO_4+Li^{comp} \leftrightarrow BO_3+NBO+Li^{mod} \quad (1)$$

where Li^{comp} and Li^{mod} refer to compensating and modifying Li ions, respectively, and NBO refers to non-bonding oxygen.

†To whom correspondence should be addressed.
E-mail: cwlee@khu.ac.kr

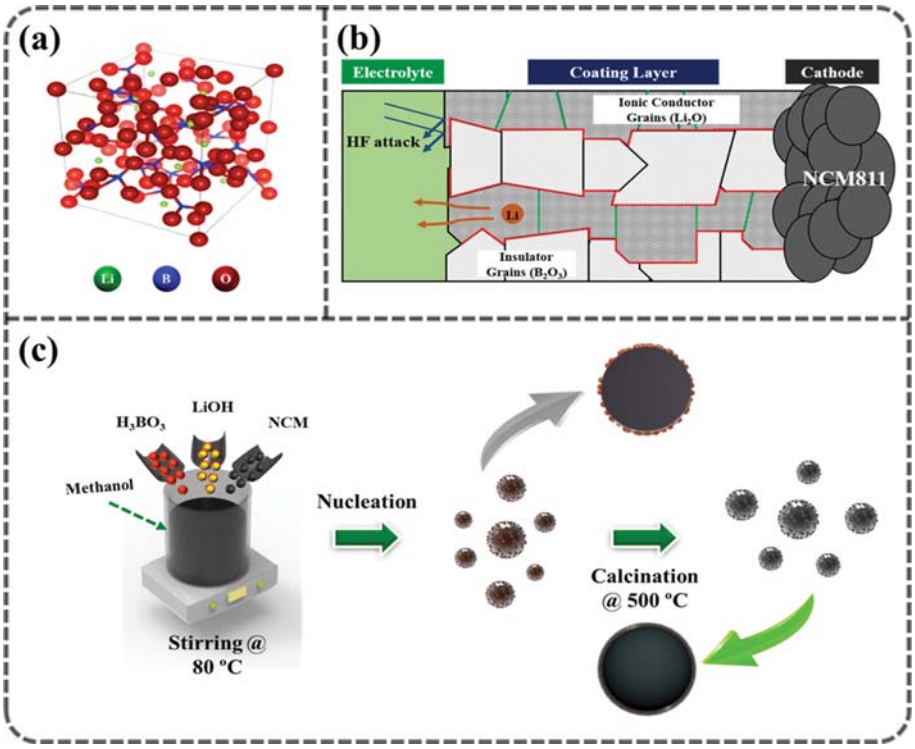

Fig. 1. (a) Schematic illustration of the random structure of Li_2O-$2B_2O_3$ glass ceramic oxide; (b) Electrochemical reaction mechanism of Li_2O-$2B_2O_3$ glass ceramic oxide coating layer and progress of Li-ion movement; and (c) Schematic illustration of synthesis process of Li_2O-$2B_2O_3$ glass ceramic oxide coating on NCM811.

In this work, an effective surface-modified Ni-rich cathode material was successfully fabricated by a wet chemical synthesis technique. The physio-chemical properties of the as-prepared Li_2O-$2B_2O_3$-coated Ni-rich cathode material were investigated, and the coating layer of Li_2O-$2B_2O_3$ over the Ni-rich cathode material was analyzed. To elucidate the electrochemical performance of the Ni-rich cathode material during charge and discharge, cycling performance and rate capability analyses were performed. The results suggest that the electrochemical performance of the Li_2O-$2B_2O_3$ coated Ni-rich cathode material was improved due to the effective surface coating of the Li_2O-$2B_2O_3$ glass ceramic oxide, which can effectively help to maintain the structural stability and electrochemical stability of the core electrode material.

EXPERIMENTAL

1. Synthesis of Li_2O-$2B_2O_3$ Glass Ceramic Oxide Coated NCM

Commercially available NCM811 powder was purchased from L&F Co. Ltd., and the other chemicals used in this work were obtained from Dae-Jung Chemicals. Li_2O-$2B_2O_3$ glass ceramic oxide coated powder was prepared by a wet chemical synthesis technique. Herein, we have adopted previously reported work with small modification [33,34]. Fig. 1(c) presents a schematic illustration of the synthesis process of the Li_2O-$2B_2O_3$-coated Ni-rich cathode materials. Primarily, anhydrous lithium hydroxide (LiOH) and boric acid (H_3BO_3) were mixed at a 1 : 2 molar ratio in methanol under stirring until it dissolved completely. NCM811 cathode active material was subsequently added into the above mixed solution and stirred continuously at 80 °C until the solution evaporated. The obtained product was then collected and calcined at 500 °C for 10 h. After cooling naturally to ambient temperature, Li_2O-$2B_2O_3$ glass ceramic oxide-coated NCM811 material was finally obtained. For comparison, we tried different surface coating ratios of 0.5 wt%, 1 wt%, and 2 wt%.

2. Physio-chemical Characterizations

The crystal structure of the bare and coating materials was analyzed by X-ray diffraction (XRD, D8 Advance, Bruker) with Cu Kα radiation in the range of 10° and 80° at a scanning rate of 6° per minute. HR Raman analysis was used to study the functional properties of bare and Li_2O-$2B_2O_3$ glass ceramic oxide-coated Ni-rich cathode materials (HR Raman microscopes, in Via) with an argon ion laser with a power of 50 mW at 514 nm. The electronic valence state and surface compositions of the bare and Li_2O-$2B_2O_3$ glass ceramic oxide-coated Ni-rich cathode materials were evaluated by X-ray photoelectron spectroscopy (XPS, MultiLab2000, Thermo VG Scientific System) with a monochromatic Al X-ray source (Al-Kα line: 1,486.6 eV). The morphology and intrinsic property of the bare and Li_2O-$2B_2O_3$ glass ceramic oxide-coated Ni-rich cathode materials were evaluated by field-emission scanning electron microscopy (HR FE-SEM, LEO SUPRA 55, Carl Zeiss) and high resolution field-emission transmission electron microscopy (HR FE-TEM, JEM-2100F, JEOL).

3. Electrochemical Measurements

A CR2032 type coin cell was used to evaluate the electrochemical performance of as-prepared positive electrodes of bare and Li_2O-$2B_2O_3$ glass ceramic oxide-coated Ni-rich cathode materials. The

cathode was made from a slurry mixture containing 80 wt% active cathode material, 10 wt% denka black as the conductive agent, and 10 wt% polyvinylidenefluoride (PVdF) as the binder in N-methyyl-2-pyrrolidone (NMP). Then, the slurry mixture was laminated over aluminium foil which acts as a current collector. The laminated electrodes were dried at room temperature for 24 h and then dried in a convection oven at 120 °C for 5 h. Then, as-prepared electrodes were cut into a disc shape with a diameter of 14 mm and vacuum dried at 120 °C for 5 h to remove remaining solvents. An argon filled glove box was used to fabricate the CR2032 type coin cell used to evaluate the electrochemical performance of the bare and Li_2O-$2B_2O_3$ glass ceramic oxide-coated Ni-rich cathode materials. The electrolyte used was 1 M $LiPF_6$ in ethylene carbonate/diethyl carbonate (EC/DEC) (1 : 1 by volume). The electrochemical performances of the bare and Li_2O-$2B_2O_3$ glass ceramic oxide-coated Ni-rich cathode materials were evaluated in the range of 3.0-4.3 V at different currents at room and high temperatures by using electrochemical analyzers (BaTester 05001, HTC and ARBIN Instruments).

RESULTS AND DISCUSSION

Fig. 1(b) shows the working principle of the electrochemical reaction mechanism of Li_2O-$2B_2O_3$ glass ceramic oxide coating material. Li_2O represents ionic conductor grains and B_2O_3 represents the insulator grains. The green lines represent the network interfaces of the ionic conductor grains and red lines denote interfaces between the ionic conductor grains and insulator grains. Li_2O-$2B_2O_3$ glass consists of B_2O_3 as a network former and Li_2O as a network modifier. Li_2O grains have high conducting interfaces and they act

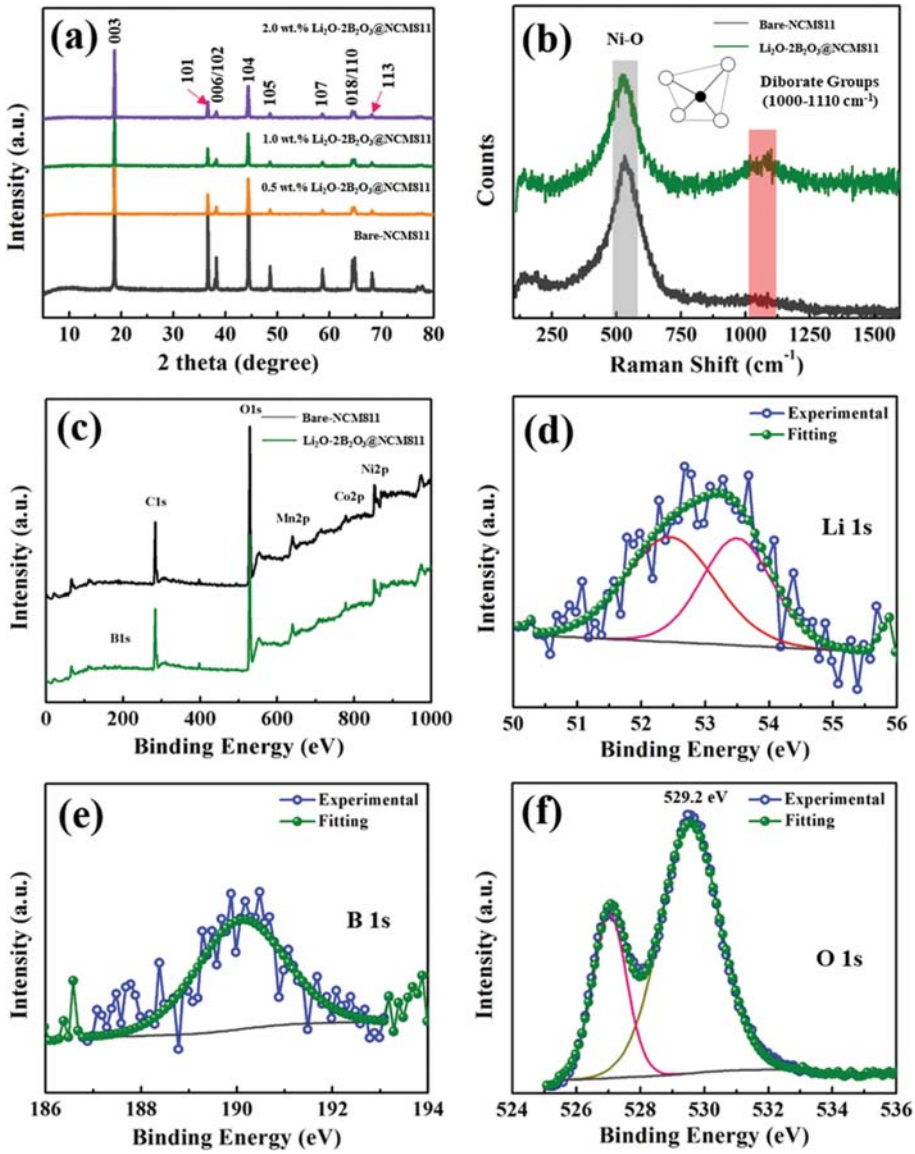

Fig. 2. (a) XRD patterns for bare and 0.5, 1.0, and 2.0 wt% of Li_2O-$2B_2O_3$ glass ceramic oxide coated NCM811; (b) Raman spectra for bare and 1.0 wt% of Li_2O-$2B_2O_3$ glass ceramic oxide coated NCM811; (c) XPS survey spectra for bare and 1.0 wt% of Li_2O-$2B_2O_3$ glass ceramic oxide coated NCM811; and (d)-(f) High-resolution XPS spectra of Li 1s, B 1s, and O 1s, respectively.

as a bridge of the pathway for Li ions [35].

Prior to evaluating the electrochemical performance, we performed physico-chemical characterizations of the bare and Li_2O-$2B_2O_3$ glass ceramic oxide-coated Ni-rich cathode materials at different ratios. Fig. 2(a) shows the XRD results for the bare and Li_2O-$2B_2O_3$ glass ceramic oxide-coated Ni-rich cathode materials with ratios of 0.5, 1.0, and 2.0 wt%. Based on the results, all the lattice parameters exactly matched the characteristic layered structure α-$NaFeO_2$ with the space group of R3m. More importantly, the doublet peaks of (006/102) at 36.7° and (018/110) at 64.3° confirmed the presence of a layered structured even after coating, signifying that the crystal structure of NCM811 is not affected with the Li_2O-$2B_2O_3$ glass ceramic oxide coating [36,37]. The functional properties were analyzed by HR Raman spectroscopy for the bare and 1.0 wt% Li_2O-$2B_2O_3$ glass ceramic oxide coated Ni-rich cathode materials, as shown in Fig. 2(b). From the results, the peak at 1,000-1,100 cm^{-1} indicates the presence of a well-defined diborate group element [38]. The chemical composition and electronic valence state of the bare and Li_2O-$2B_2O_3$ glass ceramic oxide-coated Ni-rich cathode materials were characterized by the XPS analysis and are shown in Fig. 2(c)-(f). Fig. 2(c) represents the XPS survey spectra for the bare and 1.0 wt% Li_2O-$2B_2O_3$ glass ceramic oxide-coated Ni-rich cathode materials. The survey spectra confirm the presence of elements such as Li, Ni, Co, Mn, O, B, and Si. An additional peak of silicon was obtained due to the substrate used to carry out the XPS analysis, and the dominant peak at 531 eV confirms the presence of stable metal oxide materials. Fig. 2(d) represents the core level spectrum of Li 1s, which shows two major peaks at 51.9 and 53.3 eV. Fig. 2(e) shows the deconvoluted spectrum of B 1s, which confirms the presence of a boron peak at 190.2 eV [39]. This boron peak is due to Li_2O-$2B_2O_3$ glass ceramic oxide coated over the Ni-rich cathode material surface. Fig. 2(f) depicts the core level spectrum of O 1s and the spectrum deconvoluted into two oxygen peaks at 529.5 and 530.2 eV. The peak at 529.5 eV is due to lattice oxygen in the metal framework. The peak at 530.2 eV in the O 1s spectrum, which corresponds to Li_2O-$2B_2O_3$, is also dominant in the core level spectrum of oxygen. All of the peaks are in good agreement with previously reported values, confirming that the chemical composition and electronic valence states of the Li_2O-$2B_2O_3$ glass ceramic oxide-coated Ni-rich cathode materials do not endure any alterations of the structure of the material after the coating process [40-42]. Fig. 3 represents the Fourier-transform infrared (FTIR) spectra for bare, 0.5, 1.0, and 2.0 wt% of Li_2O-$2B_2O_3$@NCM811. The vibration spectra of Ni-O, Co-O, and Mn-O are fitted into the values of 447, 512, and 576 cm^{-1}, respectively, by the normal coordinate analysis. There is an additional peak at 1,190 cm^{-1} for the samples of 0.5, 1.0, and 2.0 wt% of Li_2O-B_2O_3 and it belongs to the stretching vibration of Bi-O.

The morphological evaluation of bare and Li_2O-$2B_2O_3$ glass ceramic oxide-coated Ni-rich cathode materials was characterized by HR FE-SEM analysis, as shown in the images in Fig. 4(a)-(d)(i)-(iii) with different magnifications. From the results, all the electrode materials possess spherical particles with a size of 3-4 μm and the surfaces of the materials are very clean and smooth in all cases. From the evaluation, the outer surface of the electrode active material became rough when the coating ratio was increased. Through

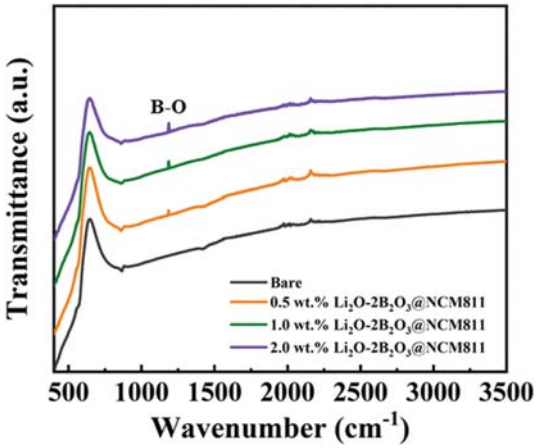

Fig. 3. FTIR spectra for bare and 0.5, 1.0, and 2.0 wt% of Li_2O-$2B_2O_3$ glass ceramic oxide coated NCM811.

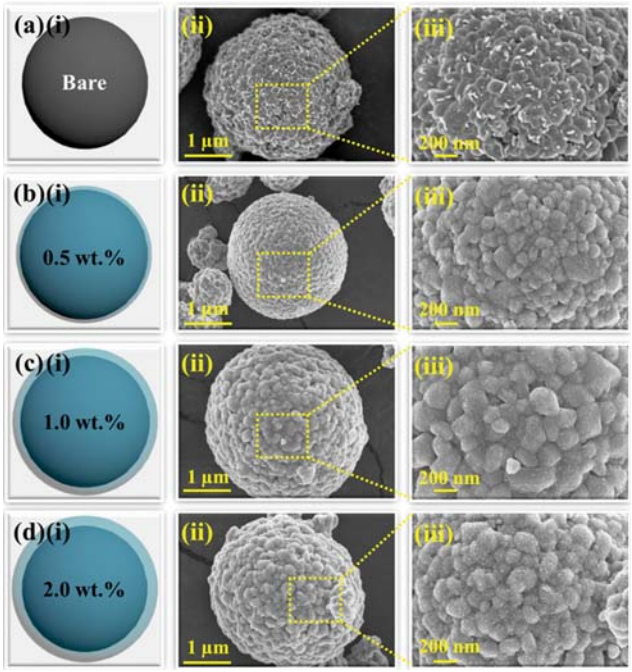

Fig. 4. (a)-(d) HR FE-SEM images for bare and 0.5, 1.0, and 2.0 wt% of Li_2O-$2B_2O_3$ glass ceramic oxide coated NCM811.

close inspection of the surface of a typical microsphere, the pores on the bare electrode active material disappeared when the coating ratio was increased. In addition, the surface binding mechanism of Li_2O-$2B_2O_3$@NCM811 could be explained that the LBO glass ceramic precursors such as LiOH and H_3BO_3 melted at 186 and 445 °C, respectively. At the time of heating process LBO glass ceramic precursors melted, reacted and then spread uniformly all over the surfaces of pristine NCM811 particles. The two strong main sources as a network modifier (Li_2O) and network former (B_2O_3) are taking the role of forming a strong glassy network structure for LBO glass ceramic coating, and these Li_2O and B_2O_3 sources are sharing some oxygen atoms which leads to the tendency of formation of oxygen vacancies. According to the Anderson-Stuart

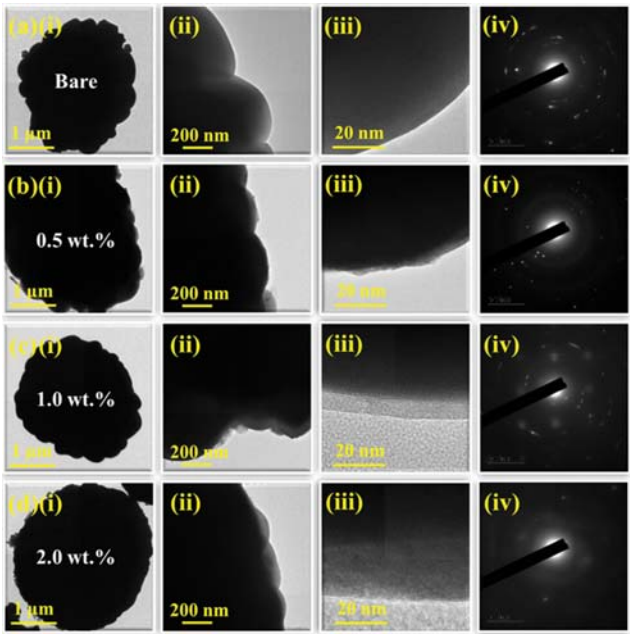

Fig. 5. (a)-(d) HR FE-TEM images for bare and 0.5, 1.0, and 2.0 wt% of Li_2O-$2B_2O_3$ glass ceramic oxide coated NCM811.

model, the Li ions progressively diffuse into the outer surface over the vacancies in the part of Li_2O. However, LBO acts as a shielding layer from the side reaction with electrolyte due to the properties of high chemical and thermal stability [43,44]. Fig. 5(a)-(d)(i)-(iv) shows the FE-TEM images for bare, 0.5, 1.0, and 2.0 wt% Li_2O-$2B_2O_3$@NCM811 at different magnifications. Fig. 5(b)-(d)(iii) confirms that a coating thickness of Li_2O-$2B_2O_3$@NCM811 increased when the coating amount of Li_2O-$2B_2O_3$ increased and the coating thickness of 1.0 wt% Li_2O-$2B_2O_3$@NCM811 is approximately 5 nm. Fig. 5(a)-(d)(iv) depicts the SAED pattern for bare, 0.5, 1.0, and 2.0 wt% Li_2O-$2B_2O_3$@NCM811, respectively. As seen from the images when the coating ratio increases, the crystalline nature of material is being moved to the polycrystalline nature, which is clearly confirmed by FE-TEM. Fig. 6(a)-(g) represents elemental mapping of 1.0 wt% Li_2O-$2B_2O_3$@NCM811 and confirms the presence of all the elements available in the material. This was further confirmed by EDS analysis as represented in Fig. 6(h).

The outstanding electrochemical performance of 1.0 wt% Li_2O-$2B_2O_3$@NCM811 was examined by obtaining the differential capacity (dQ/dV) curve in the voltage range of 3.0-4.3 V. Fig. 7((a) & (b)) shows the dQ/dV curves for bare and 1.0 wt% Li_2O-$2B_2O_3$@NCM811 at 1st, 2nd, 3rd, 5th, 10th, and 20th cycles. From the results, it can be clearly observed that both of the electrode materials have three anodic peaks at 3.758, 4.02, and 4.218 V with corresponding cathodic peaks at 3.720, 3.979, and 4.156 V, respectively, which are similar to previously reported results [45]. The polarizability in the curve for 1.0 wt% Li_2O-$2B_2O_3$@NCM811 is smaller when compared to the bare sample, which is an evidence of better electrochemical performance. To examine the electrochemical behavior of the as-prepared samples, we performed profile analysis and cycling per-

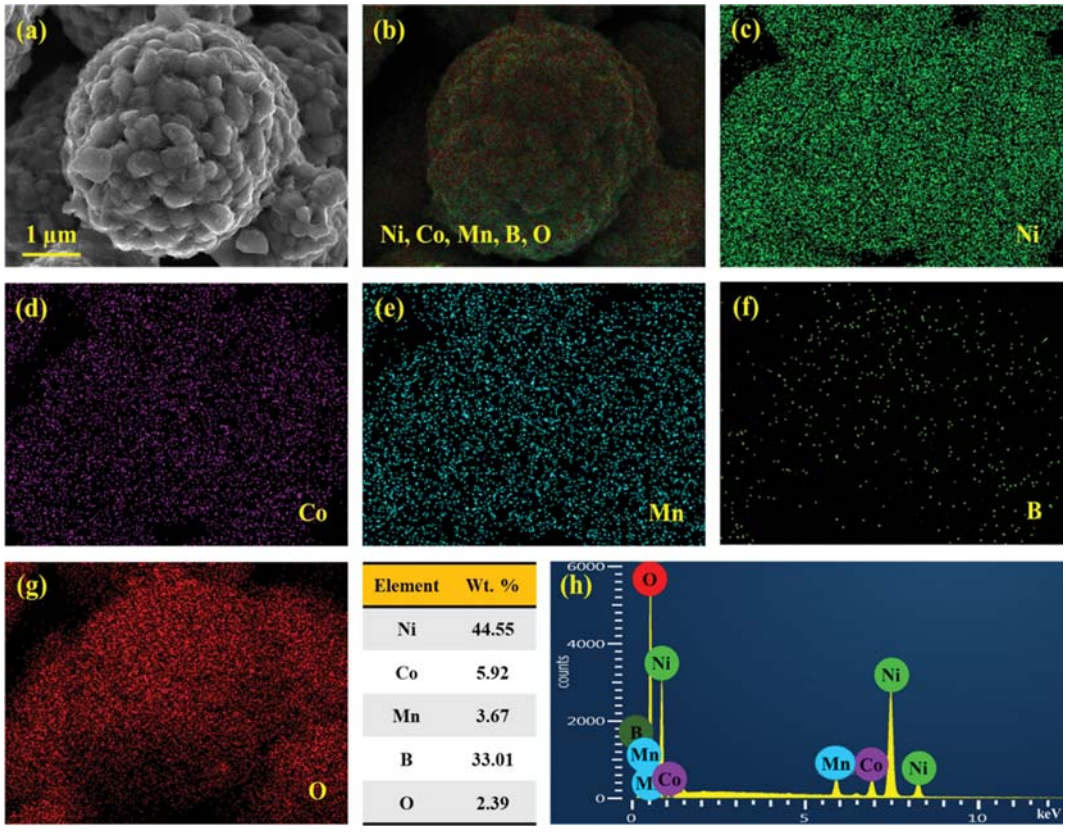

Element	Wt. %
Ni	44.55
Co	5.92
Mn	3.67
B	33.01
O	2.39

Fig. 6. (a)-(g) The elemental mapping of corresponding 1.0 wt% of Li_2O-$2B_2O_3$@NCM811 and (h) EDS analysis.

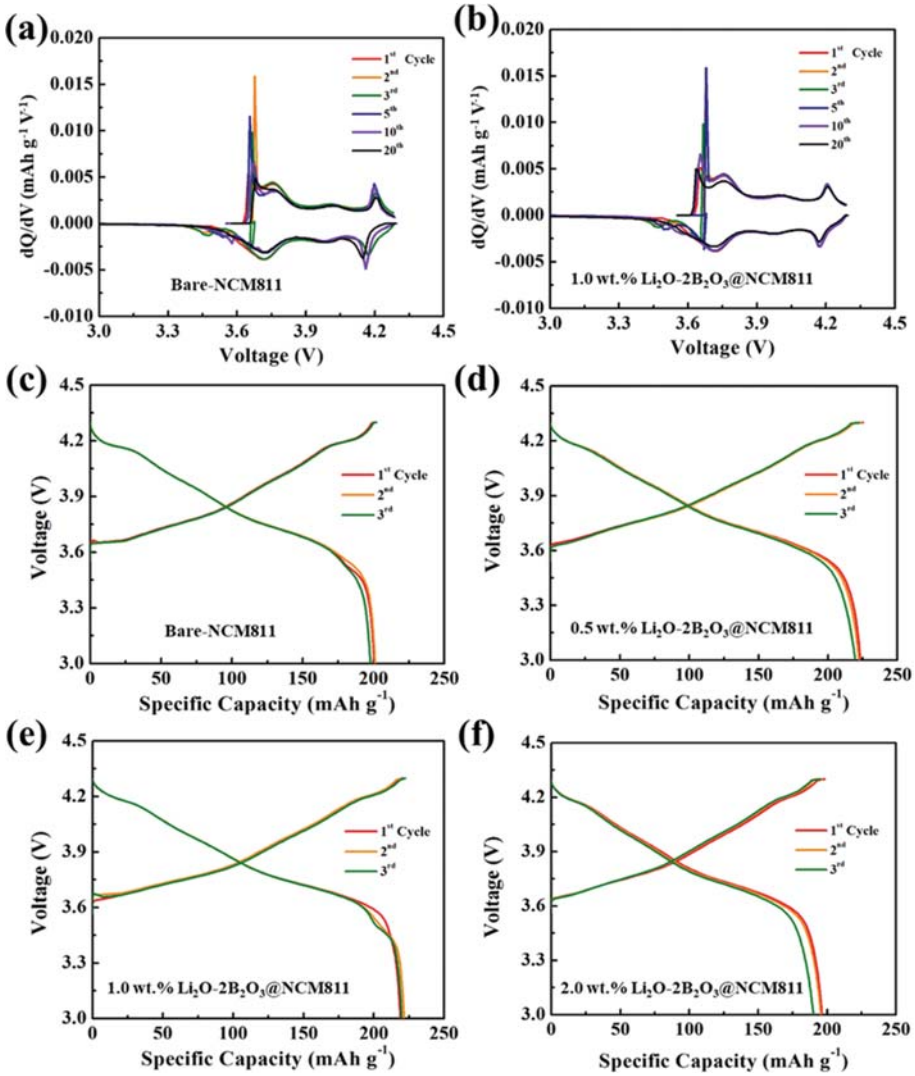

Fig. 7. (a) & (b) Differential capacity for bare and 1.0 wt% Li_2O-$2B_2O_3$ glass ceramic oxide coated NCM811 material at 0.2 C; and (c)-(f) potential profiles for bare and 0.5, 1.0, and 2.0 wt% of Li_2O-$2B_2O_3$ glass ceramic oxide coated NCM811 materials at room temperature.

formance evaluation in the voltage range of 3.0 to 4.3 V at a current rate of 0.2 C and a room temperature of 25 °C, as shown in Fig. 7(c)-(f). The results demonstrated the galvanostatic charge and discharge behaviors for the bare and 0.5, 1.0, and 2.0 wt% Li_2O-$2B_2O_3$ glass ceramic oxide coated Ni-rich cathode materials. The obtained results suggest that the initial charge and discharge capacity of the bare material was about 200.63 and 200.47 mAh g^{-1}, respectively, with a coulombic efficiency of 99.92%. However, the 0.5, 1.0, and 2.0 wt% materials delivered charge and discharge capacity of 225.31 and 223.32, 220.55 and 218.98, and 198.45 and 196.31 mAh g^{-1} with coulombic efficiencies of 99.12, 99.29, and 98.92%, respectively. In addition, the subsequent 2nd and 3rd cycles for the bare, 0.5, 1.0, and 2.0 wt% Li_2O-$2B_2O_3$ glass ceramic oxide-coated Ni-rich cathode materials show discharge capacity of 201.06 and 197.79, 222.42 and 219.58, 221.59 and 219.92, and 195.57 and 190.03 mAh g^{-1} with coulombic efficiencies of 97.93, 98.61, 98.82, and 97.26%, respectively. From these results, 1 wt% Li_2O-$2B_2O_3$ glass ceramic oxide-coated Ni-rich cathode material demonstrated the highest specific capacities. In addition, Li_2O-$2B_2O_3$ glass ceramic oxide at a loading of 1 wt% acted as a good ionic conductor and it promoted Li ion transfer between NCM811 and electrolyte. However, the 2.0 wt% Li_2O-$2B_2O_3$ glass ceramic oxide-coated Ni-rich cathode material exhibited a decreasing specific capacity, which suggests that a thicker Li_2O-$2B_2O_3$ glass ceramic oxide coating layer does not allow Li ion diffusion and leads to poor electrochemical performance.

Fig. 8(a)-(d) represents the galvanostatic cycling performance for the bare and coated materials at a current rate of 0.2 C in the voltage range between 3.0 and 4.3 V. From the results, the charge-discharge capacity of the bare material slowly decreases as cycling proceeds. At the end of the 20th cycle, the bare material galvanostatically shows a specific capacity of about 182 mAh g^{-1}, whereas the 0.5, 1.0, and 2.0 wt% materials delivered specific capacities of 150, 198, and 159 mAh g^{-1}, respectively. As known, the electrochemical performance of NCM811 is affected by different aspects like HF attack caused by anionic oxidation of PF_6^- and the dissolution

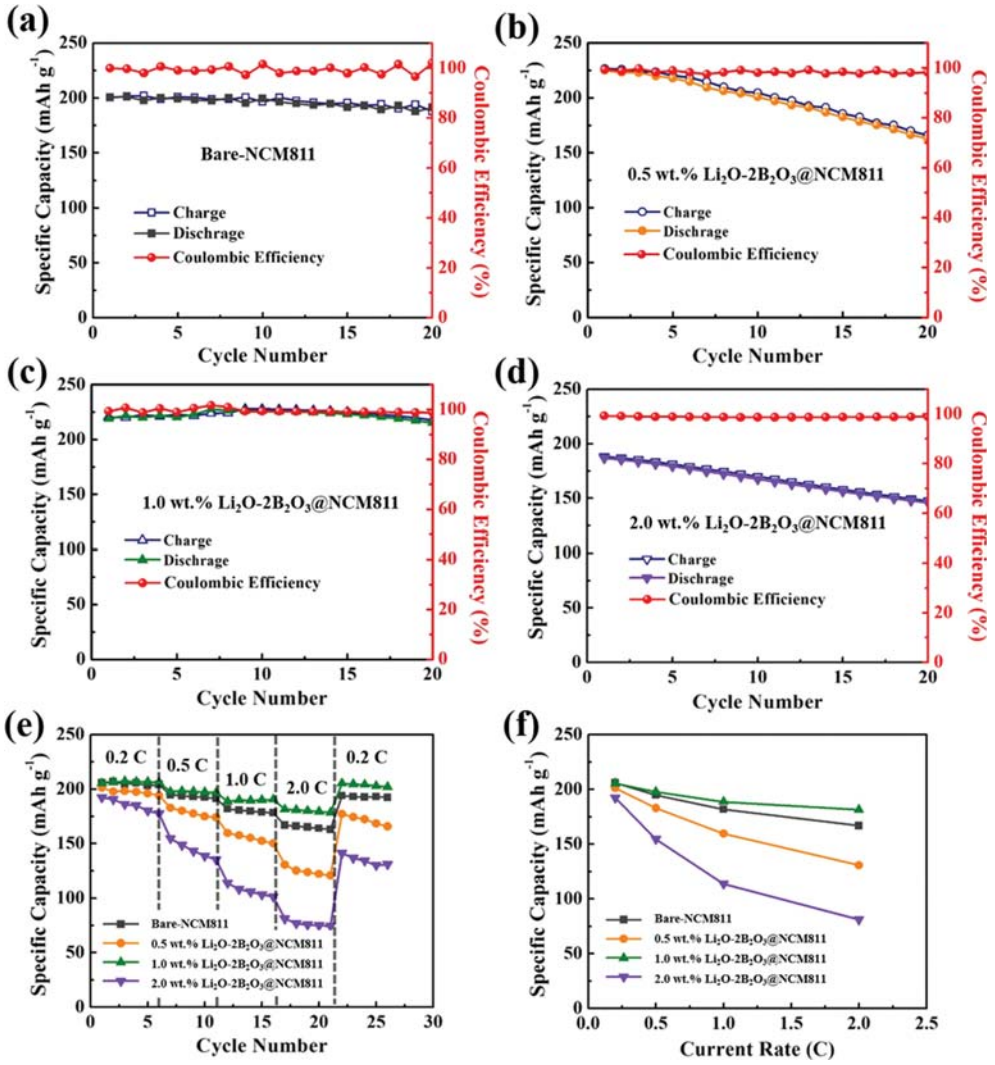

Fig. 8. (a)-(d) Cycling performance for bare and 0.5, 1.0, and 2 wt% of Li_2O-$2B_2O_3$ glass ceramic oxide coated NCM811 materials at room temperature; (e) Rate capability for bare and 0.5, 1.0, and 2.0 wt% of Li_2O-$2B_2O_3$ glass ceramic oxide coated NCM811 materials at different current rates; and (f) Specific capacity vs. current density diagram for bare and 0.5, 1.0, and 2.0 wt% of Li_2O-$2B_2O_3$ glass ceramic oxide coated NCM811 materials at different current rates.

of transition metals on the surface of the particles in charged states, which leads to capacity fading during the cycling process. The as-prepared 1.0 wt% Li_2O-$2B_2O_3$@NCM811 has higher cyclic stability when compared to the bare, 0.5 wt%, and 2.0 wt% materials. The electrode coated with 1.0 wt% demonstrated better electrochemical performance and was determined to be the optimum thickness for effective electronic and ionic transportation. The rate capability for the bare and different coated electrode materials was characterized to check the stability and performance of the as-prepared materials at different current rates in the voltage range of 3.0 to 4.3 V, as shown in Fig. 8(e). The bare and 1.0 wt% Li_2O-$2B_2O_3$ @NCM811 materials delivered higher specific capacity when compared to the 0.5 and 2.0 wt%. Li_2O-$2B_2O_3$ glass ceramic oxide-coated samples. However, when the current density increases, the specific capacity of the bare material decreases. Among the various weight percentages, 1.0 wt% Li_2O-$2B_2O_3$@NCM811 had a higher specific capacity of 180 mAh g^{-1} at a higher current density, whereas the other coating ratios such as 0.5 and 2.0 wt% showed specific capacity of 125 and 75 mAh g^{-1}, respectively, which demonstrates that 1.0 wt% coated material showed the highest stability even at higher current rates. Fig. 8(f) represents a simple comparison of the current rates vs. specific capacity. It also provides evidence that 1.0 wt% Li_2O-$2B_2O_3$@NCM811 shows better electrochemical performance compared to the bare and other coating ratio materials. Table 1 represents a comparison of charge capacity for NCM811 materials coated with various types of metal oxides, and it shows that the present work exhibits the highest capacity over the previously reported work. Therefore, a nano-sized coating layer could enhance the transport of electronics and ions to improve the rate capability of 1 wt% Li_2O-$2B_2O_3$@NCM811.

In addition, the electrochemical performance at elevated temperatures was analyzed for the bare and 1.0 wt% materials, as shown in Fig. 9((a) and (b)). Fig. 9(a) shows the initial discharge for the bare and coated materials. All charge-discharge capacities increased

Table 1. A comparison of charge capacity for NCM811 materials coated with various types of metal oxides

Sample name	Charge capacity (mAh g^{-1}) at 0.1 C current rate	Charge capacity (mAh g^{-1}) at 0.1 C current rate	References
	1st Cycle	20th Cycle	
Li_2WO_4 or WO_3@NCM811	192	179	[46]
Al_2O_3@NCM811	212	178	[47]
Li_2O-$2B_2O_3$@NCM811	220.55	198.56	This Work

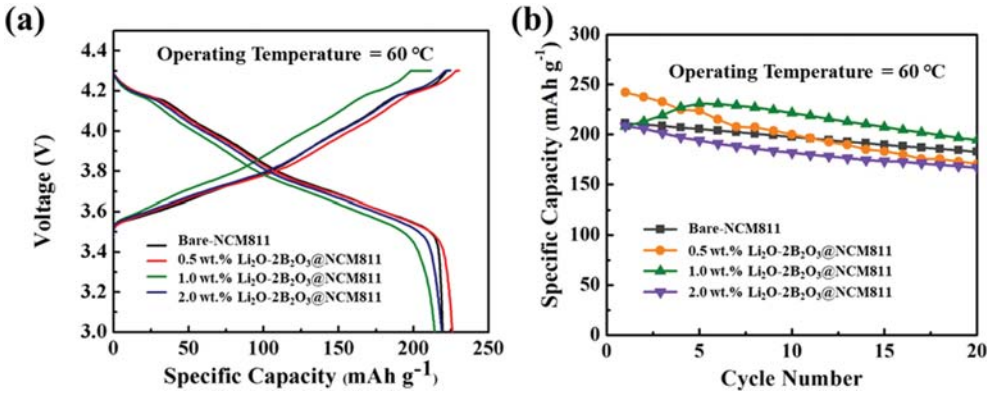

Fig. 9. (a) Potential profiles of initial charge-discharge for bare and 1.0 wt% of Li_2O-$2B_2O_3$ glass ceramic oxide coated NCM811 material at an elevated temperature, 60 °C; and (b) Cycling performance for bare and 1.0 wt% of Li_2O-$2B_2O_3$ glass ceramic oxide coated NCM811 material at an elevated temperature, 60 °C.

as cycling progressed. At elevated temperatures, electrons move to the excited states, which can increase Li ion diffusivity. Moreover, we monitored the cycling stability for 20 cycles, as shown in Fig. 9(b). The bare NCM811 showed capacity retention of about 77% and 1.0 wt% Li_2O-$2B_2O_3$ glass ceramic oxide demonstrated capacity retention of about 79% at 0.2 C. Except for the 1.0 wt% coated material, all of the other coated materials did not show good performance compared to the bare NCM811 because the other ratios have a small or large amount of Li_2O-$2B_2O_3$ glass ceramic oxide layer, which cannot prevent thermal cracks. On the other hand, the 1.0 wt% coating shows good capacity because the proper amount of Li_2O-$2B_2O_3$ glass ceramic oxide helps to increase ionic transport.

Overall, a uniform and thin glass ceramic oxide coating layer is an effective approach to improve the cyclic stability and rate capability as well as acting as an HF inhibitor and/or HF scavenger. In this work, we successfully prepared Li_2O-$2B_2O_3$ glass ceramic oxide coated NCM811 materials and understand the electrochemical enhancement of LIB performance in the voltage range of 3.0-4.3 V. The Li_2O-$2B_2O_3$@NCM811 sample possesses an insulating role of the Li_2O-$2B_2O_3$ coating layer from electrolyte.

CONCLUSION

We successfully prepared Li_2O-$2B_2O_3$ glass ceramic oxide coated Ni-rich cathode materials by a wet chemical synthesis process and used the surface modified cathode electro-active materials to enhance the capacity and thermal stability of the electrode in LIBs. The 1.0 wt% Li_2O-$2B_2O_3$ glass ceramic oxide coated Ni-rich cathode material showed a good discharge capacity and improved electrochemical performance during the cycling at ambient and elevated temperatures. These improvements of the Li_2O-$2B_2O_3$ glass ceramic oxide coating material on the surface of Ni-rich cathode material reduce not only metal-ion dissolution and lithium leaching but also the polarizability and charge transfer resistance of the electro-active materials. From these points of view, the Li_2O-$2B_2O_3$ glass ceramic oxide coated Ni-rich cathode material will play a significant role to promote the application of LIBs.

ACKNOWLEDGEMENTS

This work was supported by the National Research Foundation of Korea (NRF) grant funded by the Korean government (MSIT) (No. 2017H1D8A2031138).

REFERENCES

1. Y. K. Sun, S. T. Myung, B. C. Park, J. Prakash, I. Belharouak and K. Amine, *Nat. Mater.*, **8**, 320 (2009).
2. J. O'Heir, *Mech. Eng.*, **139**, 10 (2017).
3. L. Ji, Z. Lin, M. Alcoutlabi and X. Zhang, *Energy Environ. Sci.*, **4**, 2682 (2011).
4. J. P. Zhu, Q. B. Xu, H. W. Yang, J. J. Zhao and G. Yang, *J. Nanosci. Nanotechnol.*, **11**, 10357 (2011).
5. M. Wohlfahrt-Mehrens, C. Vogler and J. Garche, *J. Power Sources*, **127**, 58 (2004).
6. J. B. Goodenough, *J. Solid State Electrochem.*, **16**, 2019 (2012).
7. A. Manthiram and J. Kim, *Chem. Mater.*, **10**, 2895 (1998).
8. J. Fan and P. S. Fedkiw, *J. Power Sources*, **72**, 165 (1998).

9. J. Kim and A. Manthiram, *Electrochem. Solid-State Lett.*, **1**, 207 (1998).
10. K. Y. Chung and K. B. Kim, *Electrochim. Acta*, **49**, 3327 (2004).
11. K. Y. Chung and K. B. Kim, *J. Electrochem. Soc.*, **149**, 79 (2002).
12. P. R. Ilango, T. Subburaj, K. Prasanna, Y. N. Jo and C. W. Lee, *Mater. Chem. Phys.*, **158**, 45 (2015).
13. Y. N. Jo, K. Prasanna, S. J. Park and C. W. Lee, *Electrochim. Acta*, **108**, 32 (2013).
14. C. Liang, F. Kong, R. C. Longo, K. C. Santosh, J. S. Kim, S. H. Jeon, S. A. Choi and K. Cho, *J. Phys. Chem. C*, **120**, 6383 (2016).
15. L. Zhang, H. Wang, L. Wang and Y. Cao, *Appl. Surf. Sci.*, **450**, 461 (2018).
16. K. Min, S. W. Seo, Y. Y. Song, H. S. Lee and E. Cho, *Phys. Chem. Chem. Phys.*, **19**, 1762 (2017).
17. M. Dixit, B. Markovsky, F. Schipper, D. Aurbach and D. T. Major, *J. Phys. Chem. C*, **121**, 22628 (2017).
18. M. A. Mezaal, L. Qu, G. Li, W. Liu, X. Zhao, Z. Fan and L. Lei, *J. Solid State Electrochem.*, **21**, 2219 (2017).
19. M. Sathiya, G. Rousse, K. Ramesha, C. P. Laisa, H. Vezin, M. T. Sougrati, M. L. Doublet, D. Foix, D. Gonbeau, W. Walker, A. S. Prakash, M. Ben Hassine, L. Dupont and J. M. Tarascon, *Nature Mater.*, **12**, 827 (2013).
20. A. Grimaud, W. T. Hong, Y. Shao-Horn and J. M. Tarascon, *Nat. Mater.*, **15**, 121 (2016).
21. A. Abouimrane, I. Belharouak and K. Amine, *Electrochem. Commun.*, **11**, 1073 (2009).
22. J. R. He, Y. F. Chen, P. J. Li, Z. G. Wang, F. Qi and J. B. Liu, *RSC Adv.*, **4**, 2568 (2014).
23. J. H. Shim, Y. M. Kim, M. Park, J. Kim and S. Lee, *ACS Appl. Mater. Interfaces*, **9**, 18720 (2017).
24. W. Luo and B. Zheng, *Appl. Surf. Sci.*, **404**, 310 (2017).
25. S. H. Kang, Y. N. Jo, K. Prasanna, T. H. Kim, S. J. Do, P. Santhoshkumar, I. N. Sivagami and C. W. Lee, *J. Nanosci. Nanotech.*, **17**, 8093 (2017).
26. C. Senthil, K. Vediappan, M. Nanthagopal, H. S. Kang, P. Santhoshkumar, R. Gnanamuthu and C. W. Lee, *Chem. Eng. J.*, **372**, 765 (2019).
27. F. Schipper, H. Bouzaglo, M. Dixit, E. M. Erickson, T. Weigel, M. Talianker, J. Grinblat, L. Burstein, M. Schmidt, J. Lampert, C. Erk, B. Markovsky, D. T. Major and D. Aurbach, *Adv. Energy Mater.*, **8**, 1701682 (2018).
28. X. Xiong, Z. Wang, X. Yin, H. Guo and X. Li, *Mater. Lett.*, **110**, 4 (2013).
29. J. Cho, T. J. Kim, J. Kim, M. Noh and B. Park, *J. Electrochem. Soc.*, **151**, 1899 (2004).
30. W. Soppe, F. Aldenkamp and H. W. den Hartog, *J. Non-Crystal. Solids*, **91**, 351 (1987).
31. M. M. Islam, T. Bredow and P. Heitjans, *J. Phys. Condens. Matter.*, **24**, 203201 (2012).
32. O. Majérus, L. Cormier, G. Calas and B. Beuneu, *J. Phys. Chem. B.*, **107**, 13044 (2003).
33. S. Tan, L. Wang, L. Bian, J. Xu, W. Ren, P. Hu and A. Chang, *J. Power Sources*, **277**, 139 (2015).
34. S. N. Lim, W. Ahn, S.-H. Yeon and S. B. Park, *Electrochim. Acta*, **136**, 1 (2014).
35. O. Majérus, L. Cormier, G. Calas and B. Beuneu, *Phys. Rev. B - Condens. Matter Mater. Phys.*, **67**, 1 (2003).
36. M. Nanthagopal, P. Santhoshkumar, N. Shaji, S. Praveen, H. S. Kang, C. Senthil and C. W. Lee, *Appl. Surf. Sci.*, **492**, 871 (2019).
37. T. Ohzuku, A. Ueda and M. Nagayama, *J. Electrochem. Soc.*, **140**, 1862 (1993).
38. A. K. Yadav and P. Singh, *RSC Adv.*, **5**, 67583 (2015).
39. J. S. Chae, S. B. Yoon, W. S. Yoon, Y. M. Kang, S. M. Park, J. W. Lee and K. C. Roh, *J. Alloys Compd.*, **601**, 217 (2014).
40. S. Tan, L. Wang, L. Bian, J. Xu, W. Ren, P. Hu and A. Chang, *J. Power Sources*, **277**, 139 (2015).
41. S. H. Choi, J. H. Kim, Y. N. Ko, K. M. Yang and Y. C. Kang, *J. Power Sources*, **244**, 129 (2013).
42. L. Wang and Y. H. Hu, *Int. J. Energy Res.*, **43**, 4644 (2019).
43. O. Anderson and D. Stuart, *J. Am. Ceram. Soc.*, **37**, 573 (1954).
44. R. P. Rao, T. Tho and S. Adams, *Solid State Ionics*, **181**, 1 (2010).
45. S. Shen, Y. Hong, F. Zhu, Z. Cao, Y. Li, F. Ke, J. Fan, L. Zhou, L. Wu, P. Dai, M. Cai, L. Huang, Z. Zhou, J. Li, Q. Wu and S. Sun, *ACS Appl. Mater. Interfaces*, **10**, 12666 (2018).
46. D. Becker, M. Börner, R. Nölle, M. Diehl, S. Klein, U. Rodehorst, R. Schmuch, M. Winter and T. Placke, *ACS Appl. Mater. Interfaces*, **11**, 18404 (2019).
47. W. Zhu, X. Huang, T. Liu, Z. Xie, Y. Wang, K. Tian, L. Bu, H. Wang, L. Gao and J. Zhao, *Coatings*, **9**, 92 (2019).